



University of Kentucky
UKnowledge

University of Kentucky Master's Theses

Graduate School

2011

DETERMINING INTERSTELLAR REDDENING: A NEW APPROACH USING SPECTROSCOPY AND PHOTOMETRY

Syed A. Uddin

University of Kentucky, suddin@astro.swin.edu.au

[Right click to open a feedback form in a new tab to let us know how this document benefits you.](#)

Recommended Citation

Uddin, Syed A., "DETERMINING INTERSTELLAR REDDENING: A NEW APPROACH USING SPECTROSCOPY AND PHOTOMETRY" (2011). *University of Kentucky Master's Theses*. 150.
https://uknowledge.uky.edu/gradschool_theses/150

This Thesis is brought to you for free and open access by the Graduate School at UKnowledge. It has been accepted for inclusion in University of Kentucky Master's Theses by an authorized administrator of UKnowledge. For more information, please contact UKnowledge@lsv.uky.edu.

ABSTRACT OF THESIS

DETERMINING INTERSTELLAR REDDENING: A NEW APPROACH USING SPECTROSCOPY AND PHOTOMETRY

The mystery of Canis Major overdensity is addressed. We discuss concurrent methods and their limitations on the determination of interstellar reddening. We establish a new way to determine line of sight interstellar reddening by observing stellar spectral lines and UBV colors. We observe and analyze spectra of 22 stars in different open clusters. We find that Hydrogen Balmer line at 4861 angstrom can predict the stellar atmospheric parameters and intrinsic colors with reasonable accuracy. Comparing with observed colors we derive the reddening of the stars. We compare our results with standard database WEBDA and find that within 90% probability limit the standard deviation of the error is 0.102798. This is improved by taking the absolute maximum probabilities and the scatter becomes 0.0688865.

KEYWORDS: Reddening, Balmer lines, chi-square

Author's signature: _____ Syed A. Uddin

Date: _____ July 10, 2011

DETERMINING INTERSTELLAR REDDENING: A NEW APPROACH USING
SPECTROSCOPY AND PHOTOMETRY

By
Syed A. Uddin

Director of Thesis: Tom Troland

Director of Graduate Studies: Dr. Joe Brill

Date: July 10, 2011

RULES FOR THE USE OF THESES

Unpublished thesis submitted for the Master's degree and deposited in the University of Kentucky Library are as a rule open for inspection, but are to be used only with due regard to the rights of the authors. Bibliographical references may be noted, but quotations or summaries of parts may be published only with the permission of the author, and with the usual scholarly acknowledgments.

Extensive copying or publication of the thesis in whole or in part also requires the consent of the Dean of the Graduate School of the University of Kentucky.

THESIS

Syed A. Uddin

The Graduate School
University of Kentucky
2011

DETERMINING INTERSTELLAR REDDENING: A NEW APPROACH USING
SPECTROSCOPY AND PHOTOMETRY

THESIS

A thesis submitted in partial fulfillment
of the requirements for the degree of
Master of Science in the College of
Arts and Sciences at the University of
Kentucky

By
Syed A. Uddin
Lexington, Kentucky

Director: Tom Troland, Professor of Physics and Astronomy
Lexington, Kentucky 2011

Copyright© Syed A. Uddin 2011

ACKNOWLEDGMENTS

I like to thank my thesis committee for their generous support while doing this research. Special sincere thank for Dr. Ron Wilhelm of Physics and Astronomy department who has been advising me throughout the research work starting from observation and data reduction. The staffs at McDonald observatory have been generous while my stay there for getting the spectra. I also thank to all people in the department of Physics and Astronomy for their continuous support.

To my sister Syeda Hasne Ara, who has encouraged me about the wonders of the
universe

TABLE OF CONTENTS

Acknowledgments	iii
Table of Contents	iv
List of Figures	v
List of Tables	vi
Chapter 1 Introduction	1
1.1 Motivation	1
1.2 Interstellar Reddening	1
1.3 A Review on Reddening Measurements	3
1.4 Proposed Method	4
Chapter 2 Observation	7
2.1 Data Reduction	7
Chapter 3 Data Analysis	12
3.1 Profile Fitting	12
3.2 Model Spectra	12
3.3 Statistical Analysis	13
Chapter 4 Results	17
Chapter 5 Conclusions and recommendations	22
Appendix A Stellar Spectral Lines	23
Appendix B Hydrogen Balmer Series	26
Bibliography	27
Vita	28

LIST OF FIGURES

1.1	Variation of $H\beta$ line with temperatur	5
1.2	Variation of $H\beta$ line with surface gravity.	6
1.3	Error in predicting mean intrinsic color within a given temperature	6
2.1	Spectra of three different stars in IC 4665.	9
2.2	Normalization with different orders and noise for HD161370.	11
3.1	An example of Sersic fit	12
3.2	Use of Q -valuesfor constraining the models	14
3.3	Problem with Q -value	14
3.4	Behavior of Q -values. Horizontal lines are for sample stars.	15
3.5	Diagnostic diagram for the detection of HeI line.	16
3.6	Variation of equivalent widths	16
4.1	Prediction of temperatures and intrinsic colors	19
4.2	Prediction of reddening to individual stars	19
4.3	Prediction of reddening to individual stars	20
4.4	Absolute differences of reddening prediction	20
4.5	Absolute differences of reddening prediction	21

LIST OF TABLES

2.1	Sample	8
2.2	List of observed stars.	10
2.3	Spectrum Calibration lines.	10
4.1	Results from the work.	18

Chapter 1 Introduction

1.1 Motivation

Hierarchical clustering and merging are the predictions of the standard structure formation model (White and Rees 1978). Primordial fluctuations after the big bang act as the seeds for the formation of structures in the universe as we see today. As time goes on small structures merge and form bigger structures. The process is still ongoing and the presence of a number of small satellite galaxies near Milky Way is the evidence that the model is true. The first of such objects was discovered by Harlow Shapley in 1938 and a number of discoveries followed after that. Moreover the discovery of Sagittarius dwarf galaxy (Ibata et al. 1997) shows active accretion onto the Milky Way Galaxy.

Canis Major (CMa) overdensity (Lee, P. 2008) has been a dilemma within the astronomical community since its serendipitous discovery from the 2MASS survey for M-giant stars (Martin et al. 2004). Debates has been going on since its discovery to infer its true nature. Some suggest that it is just a warp of our own galaxy (Momany et al. 2004). Others claim it to be a satellite galaxy analog to Sagittarius dwarf. Whether it is a dwarf satellite galaxy of Milky Way or just a part of the disk of Milky Way is the problem to solve. The debate can be solved easily if we can determine the distance of CMa with acceptable accuracy. Accurate distance determination is crucial in this case as CMa lies close to the galactic disk and suffers from heavy differential reddening when viewed from our vantage point.

Moreover, a population of stars known as blue plume (BP) stars (Bellazzini 2004) can help us to unveil the nature of CMa. They are hot young stars at the blue part of the color magnitude diagram (CMD). Warp model cannot explain the presence of BP stars at the edge of the galactic disk. These stars are considered as the key to CMa dilemma because the M-giant stars studied in Martin et al. are at a redder end of CMD that can be easily mistaken for background red dwarf or red giants at higher distances. BP stars are relatively rare and an excess of these stars cannot be due to field contamination.

Having the above scenario, if the BP population are co-spatial with M-giants of Martin et al. then CMa can be established as a dwarf galaxy. Otherwise it will be treated as a feature of Milky Way.

Extinction and reddening caused by the interstellar dust effects the detected radiation from most astronomical sources. The problem gets even worst when objects lie close to the galactic plane. An error in determining the reddening will also produce error in distance measurement. Therefore, we aim to establish better methodology to measure reddening that will help us to remove ambiguity in reddening measurement and thus help measuring astronomical parameters of interest.

1.2 Interstellar Reddening

In astronomy, interstellar reddening is a phenomenon (associated with interstellar extinction) where the spectrum of electromagnetic radiation from a radiation source changes

characteristics from that which the object originally emitted. Dust grains in the interstellar medium have a typical size that is comparable to the wavelength of blue light. The result is that the blue light coming from distant objects is strongly absorbed and scattered by the dust, essentially removing it from the light reaching us and making the objects appear redder than they really are. This is known as interstellar reddening and must be taken into account by astronomers analyzing data taken at optical wavelengths in particular.

The reddening of an object is inversely proportional to the wavelength of optical light, so shorter wavelengths (blue) are more heavily reddened than longer (red) wavelengths. Often known as color excess reddening is essentially an extinction measured in two wavelength bands. We can determine the degree of reddening by measuring the colour index $(B - V)$ of the object and comparing that to its true or intrinsic colour index $(B - V)_0$ through the equation:

$$E(B - V) = (B - V) - (B - V)_0 = A_B - A_V \quad (1.1)$$

where A_B and A_V are the extinctions in blue and visual bands respectively. Since both interstellar reddening and extinction are the result of the interaction of starlight with dust grains, they are inextricably linked and we should expect that the more dust along the line of sight, the more pronounced the reddening and the higher the extinction. This is indeed what is found, with extinction and reddening linked by the equation:

$$A_V = R_V E(B - V) \quad (1.2)$$

where the value of $R_V \approx 3.1$. Often A_V is called total extinction and $E(B - V)$ is called selective extinction. The important role that reddening plays in astronomy is in distance measurement. In one method distance is given by :

$$d = 10^{0.5(m - M + A_V + 5)} \quad (1.3)$$

where d is the distance to be measured, m is the apparent magnitude, M is the absolute magnitude, and A_V is the extinction up to the object.

To study stellar populations or objects found throughout the galactic disk we need to know the extinction up to that stellar population or object, not the total extinction along the line of sight that certainly give us wrong values while deriving desired parameters (i.e., distances). The most recent reddening map given by Schlegel et al. (1998, hereafter SFD) is not good to study objects within the our galaxy as this reddening is based on the total extinction along the line of sight. Also presence of interstellar clouds below the resolution of this map also introduce difficulties. Attempts are also made to construct three dimensional models of the reddening maps, which also suffers from inadequate resolution of the galactic dust distribution. Therefore it is necessary to find new ways to predict reddening that will be free from above shortcomings.

In this chapter first we review some of the important studies about reddening and extinction and discuss pros and cons. Later we propose a new way to find reddening

1.3 A Review on Reddening Measurements

Reddening measurements for interstellar medium generally relies on three techniques i.e., (1) star counts, (2) spectro-photometric measurements, and (3) main sequence fitting of color-color diagram. But other tracers have also been used to study reddening. The variation of the star density across the sky was the first observable indication of the reddening (Wolf 1923). The method consists of counting stars in magnitude intervals in each cell of a regular grid in an obscured field in the sky and comparing this number with the counts in a reference field, supposedly free from absorption. It is assumed in this method that all the stars are behind the interstellar medium and the stellar population is homogeneous for the whole field. Moreover, the star density is supposed to be uniform within a cell. So, the reddening derived is also supposed to be uniform within the field.

In reality a star or stellar group can sit at any position within the interstellar medium and so the amount of reddening is only due to the clouds sitting in front of the star. Also, cloud structures (or patchiness) on angular scales smaller than the resolution of a unit field can lead to underestimate the reddening.

In spectro-photometric method reddening is derived using the observed intrinsic color. Observed color comes from the photometric observation and the intrinsic color comes from either a flux-calibrated or normalized spectra of stars. The first extensive study of extinction that utilizes spectro-photometric method was carried out by Neckel where he observed 4700 stars (Neckel 1966). Later Neckel and Klare undertook a long observing campaign where they observed 1660 stars of known spectral type (OB star) with objective prisms and photoelectric photometers (Neckel & Klare). Together with a wide number of others, mainly photoelectric UBV, MK spectral types, and $H\beta$ measurements for more than 11000 O to F star, Neckel and Klare built their extinction maps and had errors between 0.1-0.2 mag in derived extinctions.

After Neckel & Kaler's work a number of efforts has been made to measure the reddening in the sky along a line of sight and or to create a reddening map of the entire sky. Some of them allow determination of the integrated extinction up to the edge of the galaxy and thus give 2D maps. For example HI and galaxy counts (Burstein & Heiles 1978), galaxy colors (Cambresy et al. 2005), far infra red (FIR) emission (Schlegel et al. 1998). Some map the extinction at a given distance (Schultheis et al. 1999, Cambresy 2002). Other methods are improvements on the Neckel & Klare method to determine the extinction as a function of distance from photometric or spectroscopic stellar samples and to lead to 3D maps (Arenou et al. 2002). The last but not least is to turn the extinction maps into models (Drimmel & Spergel 2003).

With the advent of large digital surveys like 2MASS, statistical studies become possible where the knowledge of the spectral type is replaced by the measure of the mean color in an unobscured field. Using 2MASS prototype data, Beichman & Jarrett (1994) derived the extinction toward the Taurus cloud by comparing $J - H$ and $H - K_s$ colors to a Galactic model of stellar populations. Lada et al. (1994) proposed a method based on the $H - K$ averaged color in a regular grid to map highly extinguished clouds with visual extinction up to 30-40 mag (Alves et al. 1998; Lada, Alves, & Lada 1999). Using DENIS data, Schultheis et al. (1999) mapped the extinction toward the Galactic center with a sophisticated method based on the isochrone position in a $J - K_s / K_s$ color-magnitude diagram.

The most recent all-sky map of the galactic reddening comes from SFD. This map is based on satellite observation of FIR emission (at 100 and 250 μm) from dust. The SFD map uses data obtained from DIRBE (Diffuse Infra red Background Experiment) on board COBE (Cosmic Background Explorer) with the ISSA (IRAS Sky Survey Atlas) images. SFD used COBE data to calibrate ISSA images, and after sophisticated processing involving point source and zodiacal light removal, they obtained a full sky map of the dust at 100 μm . To transform from the map proportional to dust column (or optical depth, τ) to a reddening map, SFD use the correlation between the intrinsic B-V color of the elliptical galaxies and the Mg_2 line strength. The Mg_2 line strength of an elliptical galaxy correlates well with its intrinsic $(B - V)$ color, so that the Mg_2 line index can be used along with photometric measurements of the galaxy in order to obtain a reasonably accurate measurement of its reddening (Faber et al. 1989). SFD use a procedure where the residual of the $(B - V)$ color versus the Mg_2 line strength for 389 elliptical galaxies is correlated with the estimated reddening from their maps. The resulting fit is then used by SFD to convert from the optical depth to reddening $E(B - V)$. Finally they get the total extinction, A_v using equation (1.2).

The SFD map has a better resolution (~ 6.1 arcminutes) and accuracy than the previous all-sky reddening map of Burstein & Heiles. However, it only maps the total galactic extinction and is therefore most appropriate for extragalactic study. SFD map has been tested by Arce & Goodman (1999, AG hereafter) using four different techniques: the color excess of background stars for which spectral types are known, the ISSA 60 and 100 μm images, star counts, and optical version of color excess method used by Lada et al. (1994). All four methods gave consistent results yet different than SFD method.

In order to obtain ISSA-based extinction, AG begin by using ISSA 60 and 100 μm images to obtain a dust color temperature map from the flux ratio at each pixel. This color temperature is then used to convert the observed 100 μm optical depth. As in SFD, the next conversion, from dust opacity to extinction, is tied to a separate technique of obtaining extinction. AG chose to use a method similar to that described in Wood et al. (1994), which itself is ultimately based on work by Jarrett, Dickman, and Hetbst (1989).

Work of AG shows that, in general, SFD method gives extinction values a factor of 1.3-1.5 larger than AG. AG also conclude that SFD overestimates the reddening value to a line of sight where $E(B - V) > 0.15$ (or $A_v > 0.5$) mag. Possible explanations of this discrepancy can be found in AG paper. Moreover Bonfaccio, Monai, and Beers (Bonfaccio 2000) also report that the overestimation by SFD map also exists at lower color excess (≈ 0.10).

1.4 Proposed Method

We propose to use $H\beta$ (one of the line in Balmer series) line profile to determine the intrinsic colors of our sample stars. Balmer lines can be used like a thermometer to find the temperatures of stellar surfaces. We know we can estimate stellar temperatures from color - red stars are cool and blue stars are hot. But Balmer lines give us much greater accuracy. Also it tells us about the surface gravity of the star. These are shown in figure 1.1 and 1.2 respectively. Once we obtain the temperature with sufficient accuracy we can readily obtain intrinsic color from model data. Figure 1.3 shows the level of precision of intrinsic

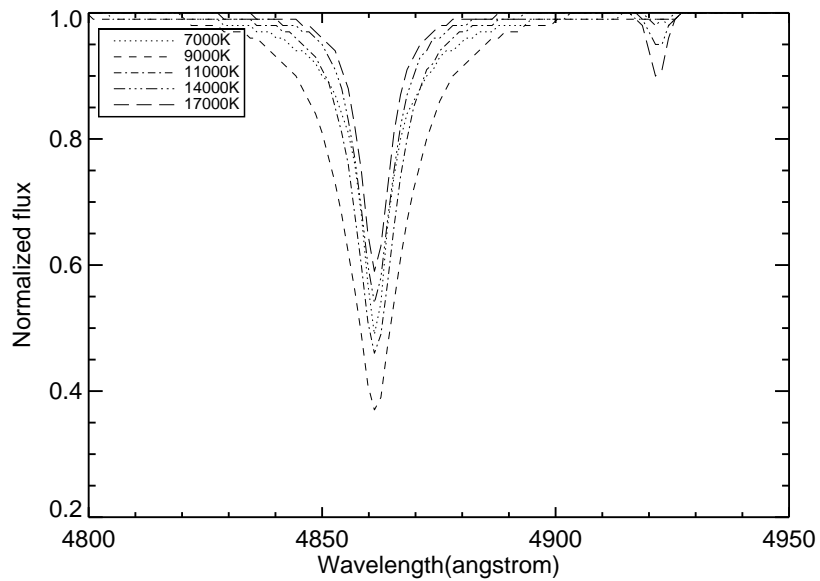


Figure 1.1: Variation of $H\beta$ line with temperature. Shown here for a model star of solar metallicity and surface gravity of 3.0. Line depth increases with increasing temperature.

color obtained from model spectra. Here we calculate the mean and standard deviation of intrinsic colors within a given temperature that includes all surface gravities and metallicities. The spread of errorbar is due to change of surface gravities and metallicities. The observed colors can be taken from previous photometry data found in databases.

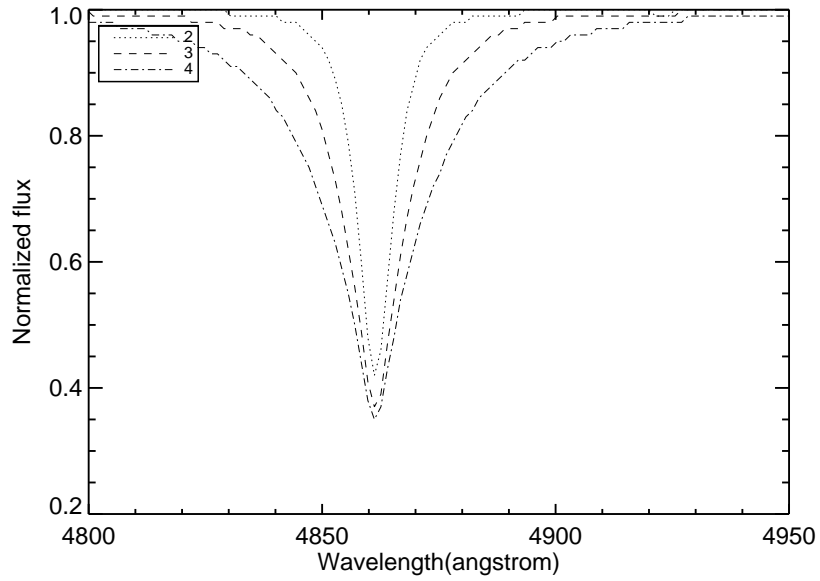


Figure 1.2: Variation of $H\beta$ line with surface gravity. Shown here for a temperature of 9000K. Higher the surface gravity wider the wing of the line.

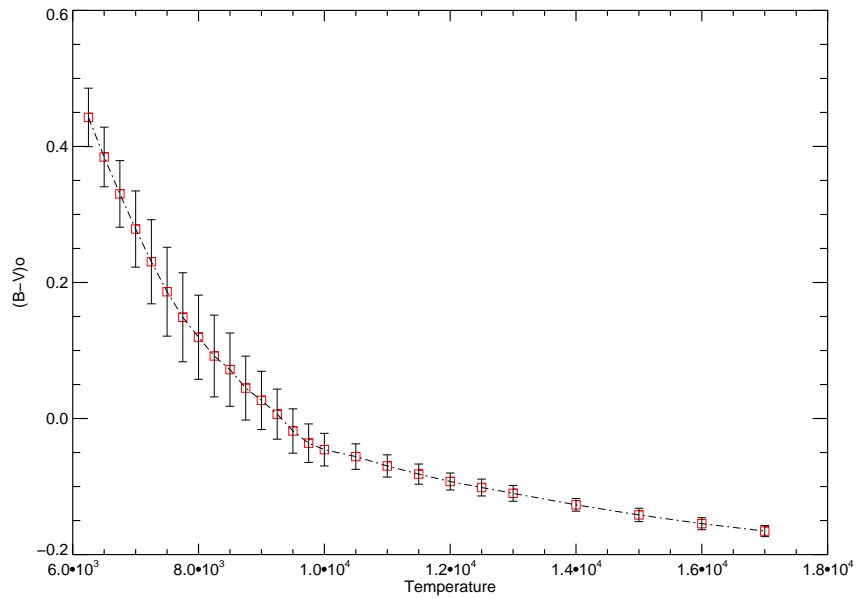


Figure 1.3: Error in predicting mean intrinsic color within a given temperature

Chapter 2 Observation

We plan to observe stars in the open clusters along the galactic disk. Since the observation condition can vary from night to night we make a list of 30 open clusters so that we can observe throughout the night and try to place them at low airmasses (towards zenith). Open clusters are selected also with varying published reddening ($E(B - V) \approx 0.0 - 0.5$). Within each cluster we try to get stars having a wide spread in intrinsic colors. We do it by subtracting the cluster reddening from the observed color. We show our initial sample in table 2.1

We were granted five observing nights with the 2.1 Otto Struve telescope at the McDonald observatory, Fort Davis, Texas from April 5-10, 2010. We use a Cassegrain spectrograph (ES2) that has a slit range from 0.5 to 120 arcseconds.. The spectrograph offers low to medium resolution with resolving power of 600-2,500 over the wavelength range from 0.3 to 1.1 micrometers. ES2 is a classic spectrometer. Light comes into the telescope, onto the primary mirror, and is reflected by the secondary mirror down to the Cassegrain focus. Within the spectrograph, the light passes through the slit, is collimated (made parallel) by reflecting off a parabolic mirror, and, then is reflected by the diffraction grating (i.e., a dispersing element) into the light's spectrum over ES2's wavelength range. This spectrum of light is then focused by a set of lenses onto the charged coupled device (CCD), either the TI1 or CC1. The TI1 CCD is used for the blue region of the spectrum (i.e. shorter wavelengths), and the CC1 CCD observes the red region (longer wavelengths).

For our observation we use a diffraction grating with 600 grooves/nm. The resolution of our system is 1300. With this we get dispersion of 1.4 angstrom/pixel. Out of five nights we were successful only three nights due to bad weather. In total we managed to get spectra of 22 stars. The observed sample is listed here (table 2.2) with information from WEBDA and SIMBAD. Spectra of three stars in IC4665 are also shown here (figure 2.1) to show the hydrogen balmer lines.

2.1 Data Reduction

Image Processing

The output that we have obtained from the spectrograph is a two dimensional dispersed image of the slit. These images contain lots of noises that originate from the instruments. Therefore we need to process them using standard image reduction methods. We have used IRAF (Image reduction and Analysis Facility) package, a general purpose software system for the reduction and analysis of astronomical data. IRAF is written and supported by the IRAF programming group at the National Optical Astronomy Observatories (NOAO) in Tucson, Arizona. In IRAF there are specific *tasks* to do specific operation. Below we describe the procedure that we use to reduce our images.

We have four types of images. Zero, flat, object, and comparison lamp. The number of zero images are same as the number of object image. We take dome flats before we begin observation. We use the task *zerocombine* to get a master zero image. Before we combine

Table 2.1: Sample

Catalog Name	Other Name	Equatorial Coordinates RA (2000) Dec	Galactic Coordinates l° b°	VMag	Diam (')	N	Distance (ly) [1] [2]
Mel 20	Alpha Per cluster	03 22.0 +49 00	146.7 -6.8	1.2	300'	50	550 600
Mel 22	M45 Pleiades	03 47.0 +24 07	166.6 -23.5	1.2	120'	100	410 490
Mel 25	Hyades	04 27.0 +16 00	180.0 -22.2	0.5	330'	40	155 150
NGC 1582	-	04 32.0 +43 51	159.3 -2.9	7.0	20'	20	- -
NGC 1647	-	04 46.0 +19 04	180.4 -16.8	6.4	40'	200	1790 1760
NGC 1746	-	05 03.6 +23 49	179.0 -10.7	6.1	42'	20	1370 2050
NGC 1893	-	05 22.7 +33 24	173.6 -1.7	7.5	11'	60	13000 10700
NGC 1912	M38	05 28.7 +35 50	172.3 +0.7	6.4	20'	100	4310 3480
Col 69	Lambda Ori clus.	05 35.1 +09 56	195.1 -12.0	2.8	65'	20	1630 1440
NGC 1980	-	05 35.4 -05 55	209.5 -19.6	2.5	15'	30	- -
Col 70	Orion's Belt	05 36.0 -01 00	205.0 -17.2	0.4	140'	100	1400 1260
NGC 1960	M36	05 36.1 +34 08	174.5 +1.0	6.0	10'	60	4140 4300
NGC 2099	M37	05 52.4 +32 33	177.7 +3.1	5.6	14'	150	4400 4510
NGC 2129	-	06 01.0 +23 18	186.6 +0.1	6.7	5'	40	6520 4940
NGC 2168	M35	06 08.9 +24 20	186.6 +2.2	5.0	25'	200	2840 2660
Col 89	-	06 18.0 +23 38	188.2 +3.7	5.7	48'	15	4240 -
NGC 2232	-	06 27.0 -04 45	214.4 -7.6	3.9	45'	20	1300 1170
NGC 2244	-	06 32.4 +04 52	206.4 -2.0	4.8	30'	100	5540 4710
NGC 2251	-	06 34.7 +08 22	203.6 +0.1	7.3	10'	30	5060 4330
Col 106	-	06 37.1 +05 57	206.0 -0.5	4.6	40'	20	- -
Col 107	-	06 37.8 +04 44	207.2 -0.9	5.1	35'	15	5540 5670
NGC 2264	Christmas Tree	06 41.1 +09 53	203.0 +2.2	3.9	40'	40	2450 2180
NGC 2281	-	06 49.3 +41 04	175.0 +17.1	5.4	25'	30	1630 1820
NGC 2323	M50	07 03.2 -08 20	221.7 -1.2	5.9	14'	80	2970 3030
NGC 2395	-	07 27.2 +13 36	204.6 +14.0	8.0	13'	30	3910 1670
NGC 2632	M44 Praesepe	08 40.1 +19 59	205.5 +32.5	3.1	70'	50	590 610
NGC 2682	M67	08 50.4 +11 49	215.6 +31.7	6.9	25'	200	2350 2960
Mel 111	Coma star cluster	12 25.0 +26 00	222.3 +84.0	1.8	120'	80	280 310
IC 4665	-	17 46.3 +05 43	30.6 +17.1	4.2	70'	30	1400 1150
Col 359	-	18 01.1 +02 54	29.8 +12.5	3.0	240'	40	650 810

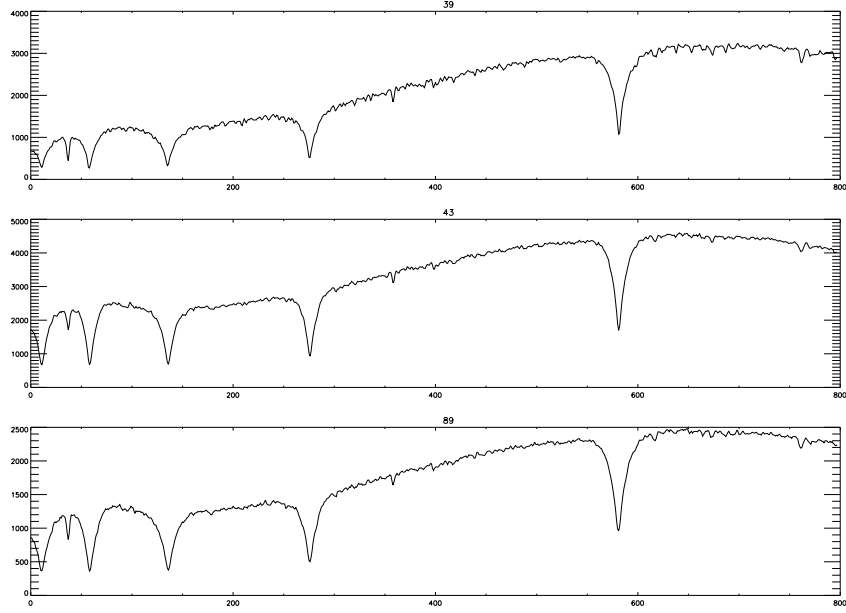


Figure 2.1: Spectra of three different stars in IC 4665. Balmer series is clearly shown starting with $H\beta$ from far right.

the flat images it is important to process all flats to get rid of bias. The task needed is *ccdproc*. Then we use *flatcombine* to get a master flat image. After that we normalize the master flat so that it reduces instrumental effects using the task *response*. After making the master zero and master flat images we process object and comparison lamp images. Now we use the same *ccdproc* and use the master zero and normalized flat images.

Spectrum extraction

The IRAF task *apall* is used for extracting one dimensional spectra. Here for each object we use the corresponding comparison lamp image. When the extractions are done we do the wavelength calibration. This is one of the most important part of data reduction. We first mark few lines knowing there wavelength beforehand and place them with the corresponding pixels. From our data we chose four standard absorption lines as shown in table 2.3

We fit the above points and find a linear fit described by the equation:

$$Y = 5225.9 - 1.7 \times X \quad (2.1)$$

We use tasks *identify* and *reidentify* do the wavelength calibration. Doing so, first we use the task *identify* to mark few lines by hand using the above formula and looking at the standard spectral atlas (in this case we use *HeNeAr* spectrum from Kitt Peak). Then we hit the library to mark more lines. We here take care of the rms values and try to keep around 20% by reducing some highly deviated points. Then we use *reidentify* to make

Table 2.2: List of observed stars. (B-V) color is taken from SIMBAD and all others are from WEBDA.

Cluster(Star)	Star Designation	(B-V)	MK-type
NGC 1746(3)	HD284937	0.194	B9
NGc 1746(4)	ASCC25751131	0.388	-
NGc 2244(348)	HD259480	0.150	B7III/B8
NGC 2244(376)	HD258691	0.570	O9V
NGC 2632(265)	HD73666	0.010	A0III/A1V
NGC 2632(348)	HD73819	0.165	A6IV/V
NGC 2632(328)	HD73785	0.200	A9III/IV-V
Mel 111(146)	HD108662	-0.050	A1/A9/B9p/A0
Mel 111(89)	HD107655	-0.020	A1III/A0V
Mel 111(130)	HD108382	0.070	A4/A3IV/A2V/F0III
Mel 111(79)	HD107427	0.110	A3V/A4III/A2V/A3V
mel 111(166)	HD109030	0.030	A0P/A0 Sr
IC 4665(39)	HD161370	0.301	A2V/A1V/A5
IC 4665(43)	HD161426	0.168	A0V/A1IV-V
IC 4665(89)	HD161786	0.234	A2V
NGC 1647(3)	HD286016	0.320	B75IV
NGC 1647(10)	HD286007	0.480	B75IV
NGC 1647(13)	HD284843	0.540	A3 V
NGC 1893(368)	HD34841	0.560	-
NGC 2099(73)	IDS05457N3233	0.488	-
NGC 2099(76)	TYC22410-0898-1	0.417	-
NGC 2168(160)	HD252318	0.220	-

Table 2.3: Spectrum Calibration lines.

Line	Wavelength (A°)	Pixel position
CaIIK	3933	759
H δ	4101	659.97
H γ	4340	518.252
H β	4861	214.6

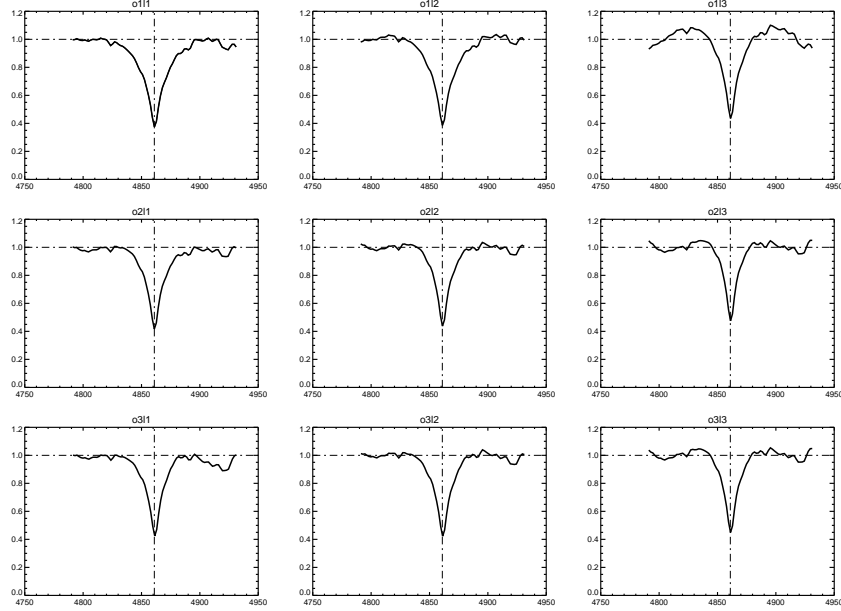


Figure 2.2: Normalization with different orders and lower limit of noise HD161370. Orders 1-3 goes from top to bottom and noise rejection goes from left to right

precise marking. At this point we need change headers of object files to assign calibration lines by using the task *refspec*.

We must have list where each object file is assigned with respective comparison lamp file. Now the wavelength solution using the desired dispersion is done using the task *dispcor*. We can also choose the range of wavelengths within which we want our spectra.

Since we have multiple exposures for a given star we need to combine them to get a single spectrum. We use the task *scombine* to combine multiple spectra into a single one. We must put gain and noise information of the instrument.

Finally we normalize our spectra since we are not doing absolute flux calibration using standard stars. Fitting continuum is one of the challenge in doing spectroscopy. We need to play with different free parameters in order to get a very close approximation. For a single object we can vary those parameters and get a set of continuum fit. This will then give us an assessment of the bounds while reducing the final result. In IRAF we use the task *continuum* to fit a continuum. We vary the *order* of the spline and *noise rejection* in σ . For each star we create nine different normalized spectra using nine ($3 \times 3 = 9$) combinations of order and low rejection. We also investigate which normalization looks good (by eye inspection). It turns out that 3σ noise reduction do not give a good continuum. An example for the star HD161370 is shown in figure 2.2

Chapter 3 Data Analysis

3.1 Profile Fitting

Since the observed data are not smooth we fit a curve that closely matches the observed line profile. $H\beta$ line-shape depends on temperature and surface gravity. Instead of Gaussian we find that the Sersic profile matches very well for our sample. The profile function is (Clewley et al. 2002) :

$$y = 1.0 - a \exp\left[-\left(\frac{|x - x_0|}{b}\right)^c\right] \quad (3.1)$$

There are four free parameters in the Sersic fit: line center, line depth, line width, line shape. We need to make an initial guess of these parameters. Then a chi-square fit will produce the best fit values for the given data. We have used the package *mpfit* to perform the chi-square fit with the Sersic profile. The line centre values are to be used for wavelength shifts due to radial velocity. An example of a fit is shown in figure 3.1.

3.2 Model Spectra

We use a set of model spectra to compare our observed spectra in order to derive the best atmospheric parameters and thereby the intrinsic colors. A set of model spectra that we use in this research taken from Kurucz stellar atmospheric models (Kurucz 1993). Model spectra are generated using the package SPECTRUM (Gray 2008). They are regenerated with

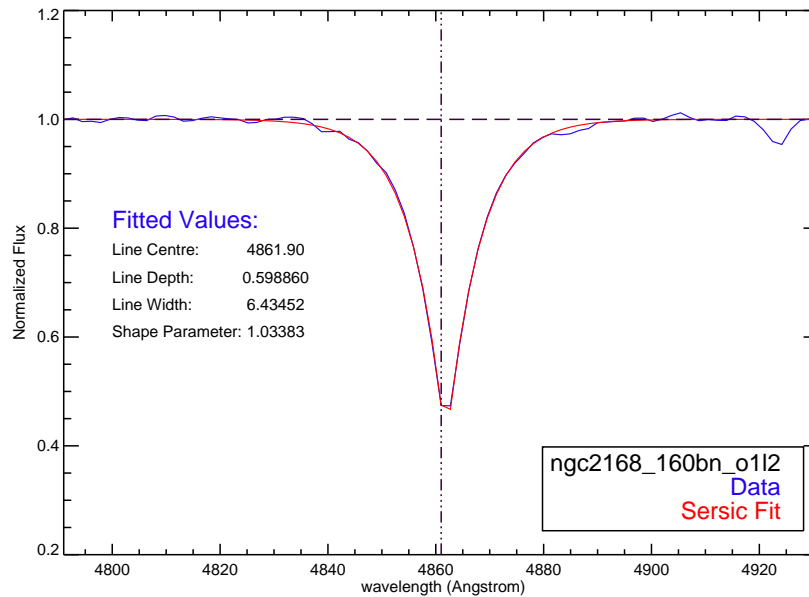


Figure 3.1: An example of Sersic fit

required dispersion (1.4 angstrom/pixel) and wavelength range. We generated model spectra for a temperature range from 6000K to 17000K. Up to 10000K the grid separation is 250K, up to 13000 it is 500K, and thereafter it is 1000K. Surface gravities (in logarithm scale) range from 2.0 to 4.5 with 0.5 increment. Metallicities (in logarithm scale) run from 0.0 to -3.0. We also construct a database for all model spectra with corresponding atmospheric parameters, colors and a reddening free parameter, Q , which is defined as :

$$Q = (U - B) - 0.72(B - V) \quad (3.2)$$

3.3 Statistical Analysis

We compare the observed spectra with the model spectra. This is done through a pixel by pixel comparison using chi-square analysis. Spectrum of a given star is compared against all 1029 model spectra and the reduced χ^2 - values is recorded. It is defined as:

$$\chi^2 = \frac{1}{N} \left(\frac{f_s - f_m}{\sigma} \right)^2 \quad (3.3)$$

Here N is the numbers of parameters, f_s and f_m are the fluxes of observed star and model star in a pixel, and σ is the noise in the spectrum (calculated from the continuum). We also calculate probabilities for each χ^2 value where probability P defined as :

$$P = e^{-\chi^2/2} \quad (3.4)$$

For each star and for a particular continuum fitting we generate a file that contains 1029 rows and contain χ^2 -values, P -values, atmospheric parameters, intrinsic color, and Q -values.

In general for a given sample spectra the atmospheric parameter corresponding to the minimum chi-square value should provide the correct stellar model for that particular spectra. But due to the degenerate nature of $H\beta$ line we just cannot take to global minimum as there are also local minimums present. We try to solve this problem in different ways.

We first constrain the models using observed Q -value for that star. The observed Q -values come from observed $(U - B)$ and $(B - V)$ colors.

The photometric values are taken from SIMBAD database and we set the standard photometric uncertainties of 1% in both U-B and B-V. So, the resulting uncertainties in Q is 1.4%. This is good enough to take care of the photometric resolution in the model spectra. We do a mapping on the probabilities based on Q -values. For a given statistical result we take only those probabilities that are within the observed Q -values. An example of using Q -values is shown in figure 3.2.

Q -values cannot sharply define the temperature. There remain bi-modalities in atmospheric parameters (see figure 3.3. The origin of this lies on the behavior of Q with temperature as shown in figure 3.4.

So, we use neutral Helium absorption line, HeI to remove bi-modality. It is a fact that HeI can only be seen in the spectra of hot stars (e.g., O and B stars). So, the detection of HeI in the spectra can serve as bisector between high and low temperatures. We look at the model spectra and see at what temperature HeI is very weak and also notice the

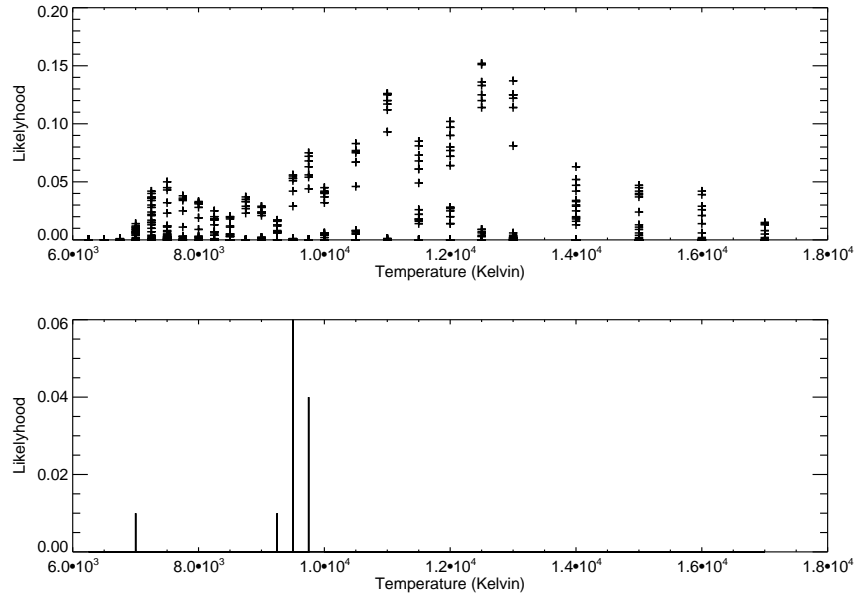


Figure 3.2: Use of Q -values for constraining the models. Upper plot shows the probabilities after performing χ^2 -test. Bottom plot shows that most of the models vanish while we use Q -value.

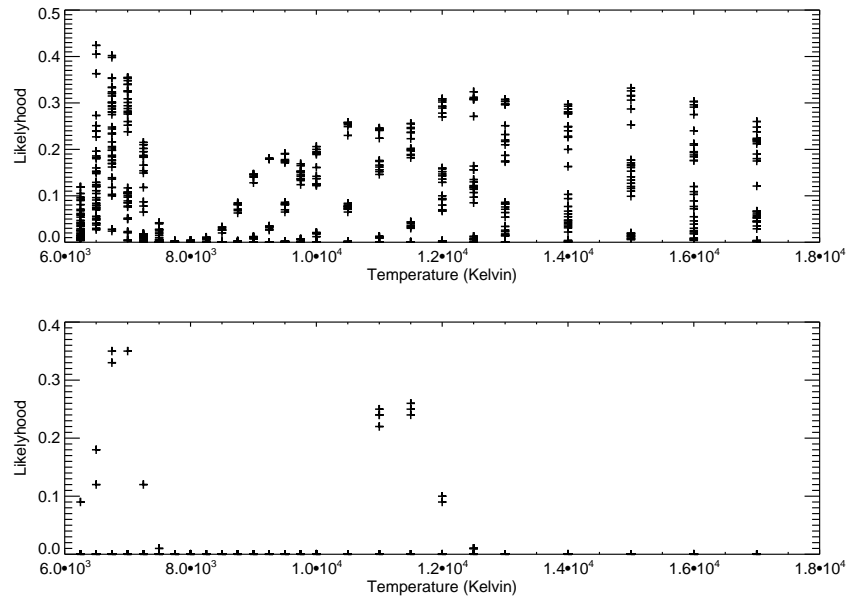


Figure 3.3: An example where Q -value cannot break the temperature bi-modality (HD032537). Some models match in the low temperature region and some at the high temperature region.

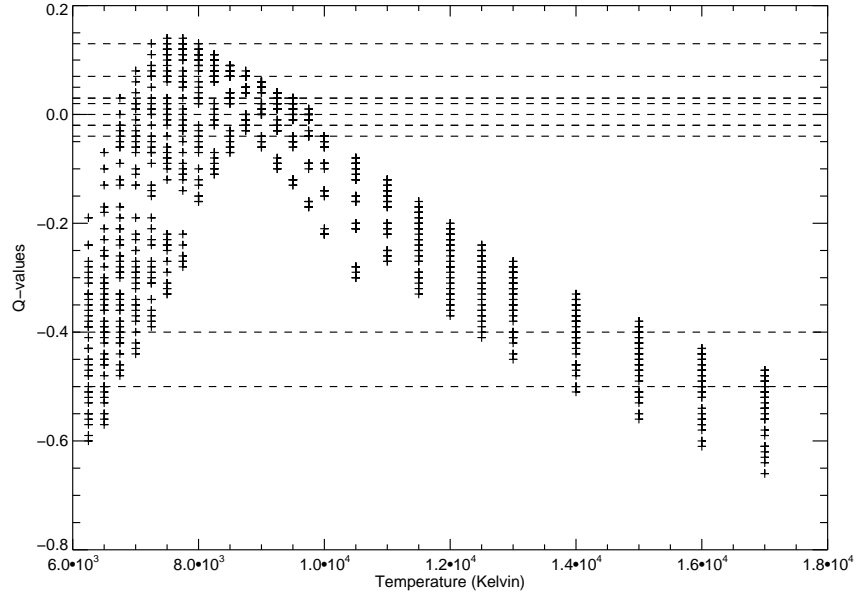


Figure 3.4: Behavior of Q -values. Horizontal lines are for sample stars.

wavelengths. Spectra of metal poor stars are useful in this regards as HeI line is not contaminated by other metal lines. Analyzing the spectra we find the threshold level of detecting HeI is at $\sim 9000K$ with the corresponding cut-off wavelength of 4470.50 \AA . We set this point where the equivalent width is $\sim 1.5\%$ of the continuum (figure 3.5). Beyond this point HeI do not exist and as the metallicity increases the equivalent widths also increases and the nominal wavelength also shifts to the blue end (figure 3.6).

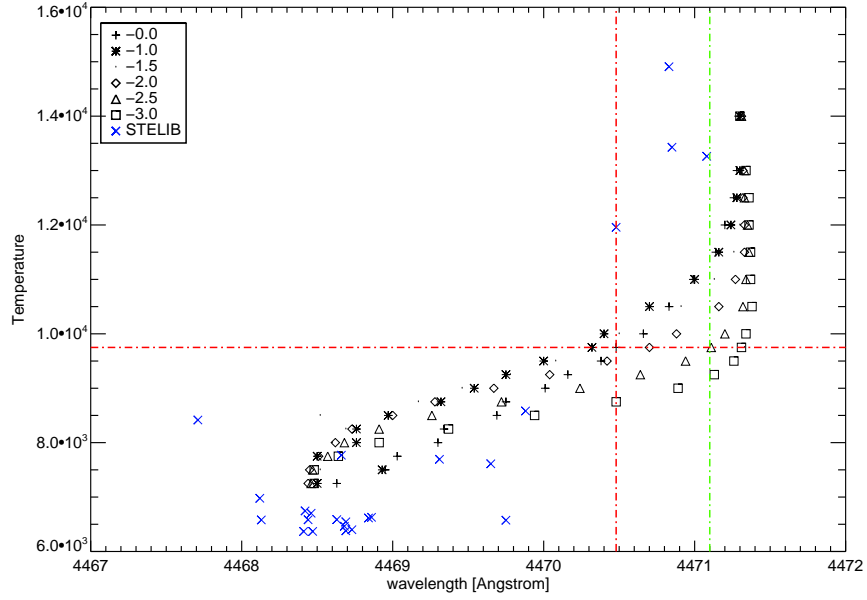


Figure 3.5: Diagnostic diagram for the detection of HeI line. We find a cutoff wavelength of 4470.48 \AA at T_{eff} of 9750K

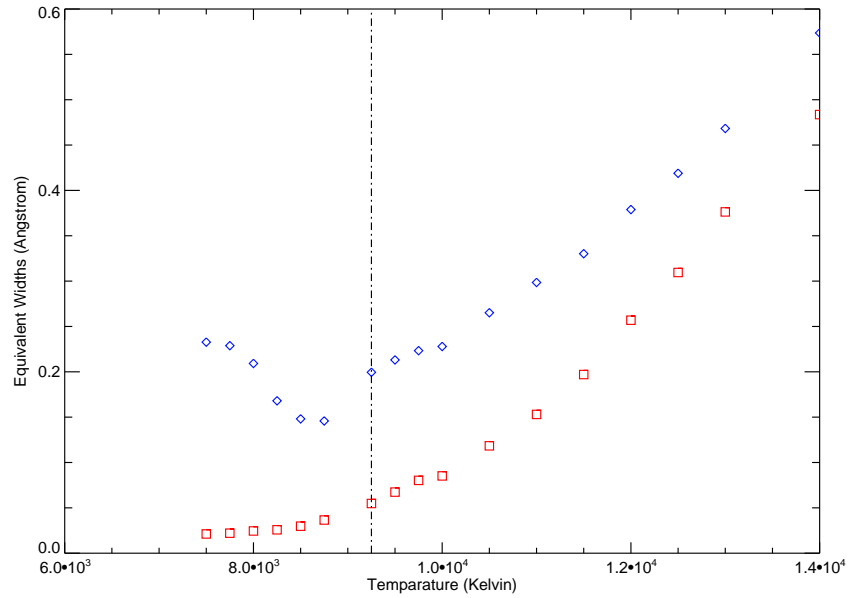


Figure 3.6: Variation of equivalent widths for metal poor (bottom curve) and solar type (top curve) metallicity.

Chapter 4 Results

We derive atmospheric parameters and intrinsic colors of our sample using χ^2 analysis and looking at the corresponding probabilities. We use spectra which are normalized with a linear spline function with 1σ noise rejection. Since temperature is the major contributor for H β line we take all the probabilities that are within 90% of the peak values. We read the corresponding intrinsic color and using the published observed color we deduce the reddening to the star. The results are shown in the following table and figures.

In the table 4.1 the first column show the cluster name and within the parenthesis is the star number from WEBDA database, second column shows the χ^2 probabilities, next three columns show all three atmospheric parameters, next two show the intrinsic colors and observed colors, eighth column show the reddening that we predict, next is the reddening from WEBDA for the respective clusters. Finally the last column show the difference between two redeningings.

In figure 4.1 we show the intrinsic colors and temperatures of all our observed stars. These are shown within 90% probabilities of χ^2 -values. For some stars we can have multiple values. Figure 4.2 and 4.3 show the derived reddening with error bars for 90% and maximum probabilities respectively. Finally figure 4.4 and 4.5 show the absolute differences of reddening predictions for 90% and maximum probabilities respectively.

The overall scatter of predicting reddening within 90% of the maximum probability is 0.102798. This is improved by taking the absolute maximum probabilities and the scatter becomes 0.0688865.

Table 4.1: Results from the work.

Star	$P(\chi^2)$	T_{eff}	Log(g)	[Fe/H]	$(B - V)_o$	$(B - V)$	$E(B - V)_s$	$E(B - V)_w$	$\Delta E(B - V)$
IC4665 (89)	0.050	9500.00	3.00	-1.50	-0.04	0.234	0.274	0.174	-0.100
IC4665 (89)	0.050	9500.00	3.00	-2.00	-0.04	0.234	0.274	0.174	-0.100
IC4665 (89)	0.050	9500.00	3.00	-2.50	-0.04	0.234	0.274	0.174	-0.100
IC4665 (89)	0.050	9500.00	3.00	-3.00	-0.04	0.234	0.274	0.174	-0.100
Mel111 (146)	0.720	7500.00	3.00	-0.00	0.20	-0.050	-0.250	0.013	0.263
Mel111 (146)	0.790	7750.00	3.00	-0.50	0.13	-0.050	-0.180	0.013	0.193
Mel111 (146)	0.780	7750.00	3.00	-1.00	0.13	-0.050	-0.180	0.013	0.193
Mel111 (146)	0.730	7750.00	3.00	-1.50	0.12	-0.050	-0.170	0.013	0.183
Mel111 (146)	0.720	8000.00	3.00	-3.00	0.09	-0.050	-0.140	0.013	0.153
Mel111 (146)	0.720	8500.00	3.00	-3.00	0.04	-0.050	-0.090	0.013	0.103
Mel111 (146)	0.800	8750.00	3.00	-0.00	0.02	-0.050	-0.070	0.013	0.083
Mel111 (146)	0.770	8750.00	3.00	-0.50	0.02	-0.050	-0.070	0.013	0.083
Mel111 (146)	0.730	8750.00	3.00	-1.00	0.02	-0.050	-0.070	0.013	0.083
Mel111 (146)	0.720	8750.00	3.00	-1.50	0.02	-0.050	-0.070	0.013	0.083
Mel111 (89)	0.190	10000.00	4.00	-0.50	-0.03	-0.020	0.010	0.013	0.003
Mel111 (130)	0.450	7750.00	3.00	-0.50	0.13	0.070	-0.060	0.013	0.073
Mel111 (130)	0.490	7750.00	3.00	-1.00	0.13	0.070	-0.060	0.013	0.073
Mel111 (130)	0.490	8750.00	3.00	-0.00	0.02	0.070	0.050	0.013	-0.037
Mel111 (79)	0.310	7500.00	3.00	-0.50	0.18	0.110	-0.070	0.013	0.083
Mel111 (79)	0.290	9500.00	3.50	-0.00	-0.03	0.110	0.140	0.013	-0.127
Mel111 (166)	0.530	9250.00	3.50	-0.00	0.00	0.030	0.030	0.013	-0.017
Mel111 (166)	0.500	9250.00	3.50	-0.50	0.00	0.030	0.030	0.013	-0.017
NGC2099 (73)	0.560	7750.00	2.50	-0.00	0.12	0.488	0.368	0.302	-0.066
NGC2099 (73)	0.570	7750.00	2.50	-0.50	0.10	0.488	0.388	0.302	-0.086
NGC2099 (73)	0.550	8000.00	2.50	-0.00	0.08	0.488	0.408	0.302	-0.106
NGC2099 (73)	0.520	8000.00	2.50	-0.50	0.07	0.488	0.418	0.302	-0.116
NGC2099 (76)	0.390	7500.00	3.50	-0.50	0.22	0.417	0.197	0.302	0.105
NGC2632 (265)	0.500	9500.00	3.50	-0.00	-0.03	0.010	0.040	0.009	-0.031
NGC2632 (265)	0.480	9500.00	3.50	-0.50	-0.02	0.010	0.030	0.009	-0.021
NGC2632 (324)	0.750	7250.00	3.00	-0.00	0.26	0.200	-0.060	0.009	0.069
NGC2632 (348)	0.620	7500.00	3.00	-0.50	0.18	0.165	-0.015	0.009	0.024
NGC2168 (160)	0.050	14000.00	3.50	-1.00	-0.13	0.220	0.350	0.262	-0.088

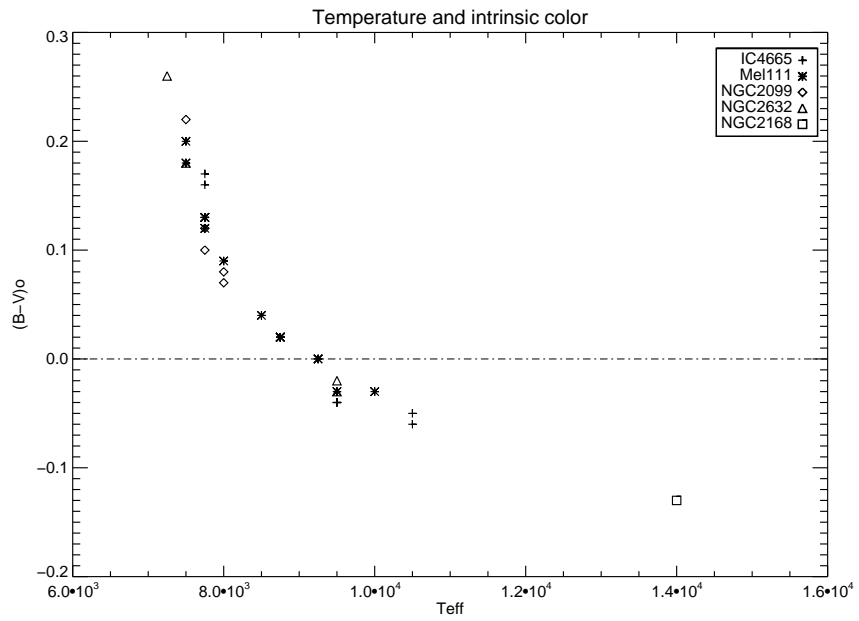


Figure 4.1: Prediction of temperatures and intrinsic colors

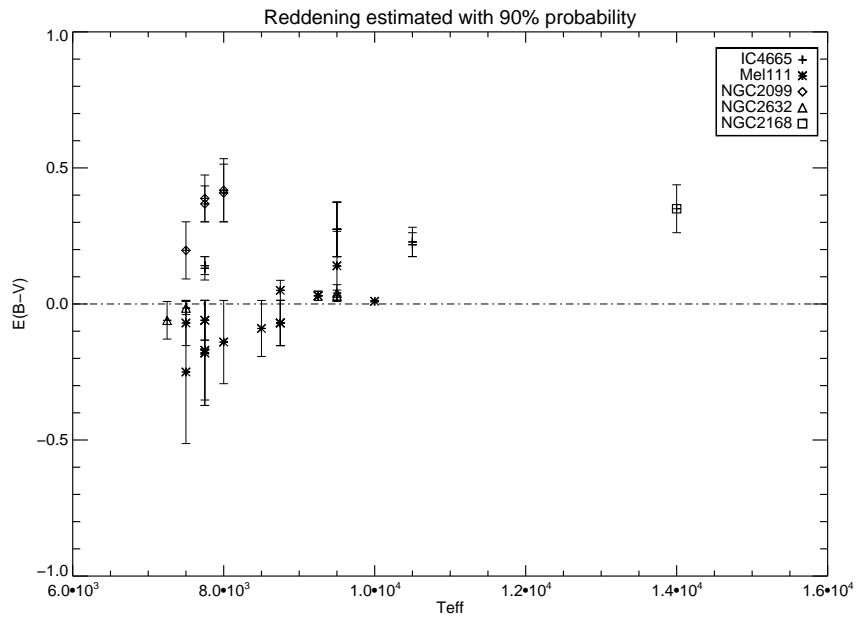


Figure 4.2: Prediction of reddening to individual stars. Error bars are the difference with WEBDA values for the respective clusters.

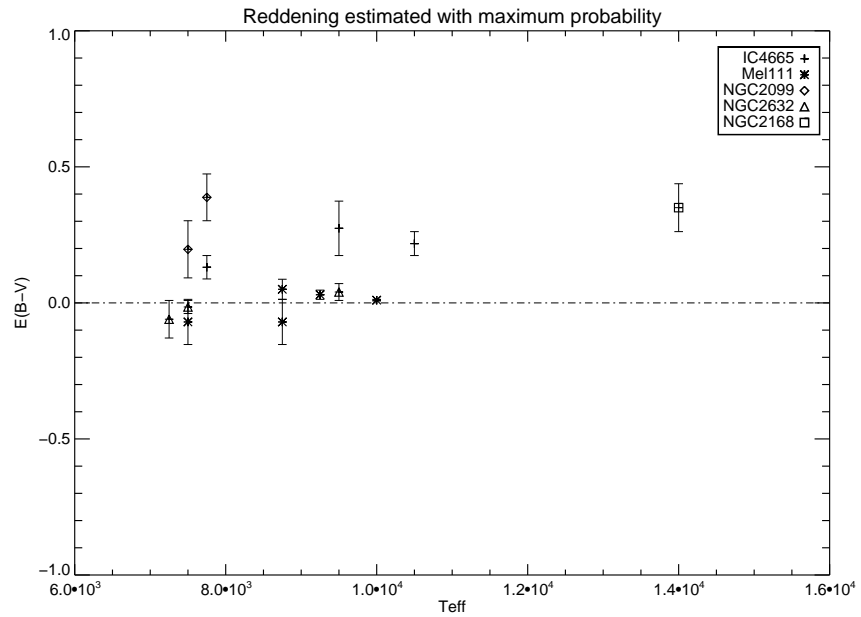


Figure 4.3: Prediction of reddening to individual stars. Error bars are the difference with WEBDA values for the respective clusters.

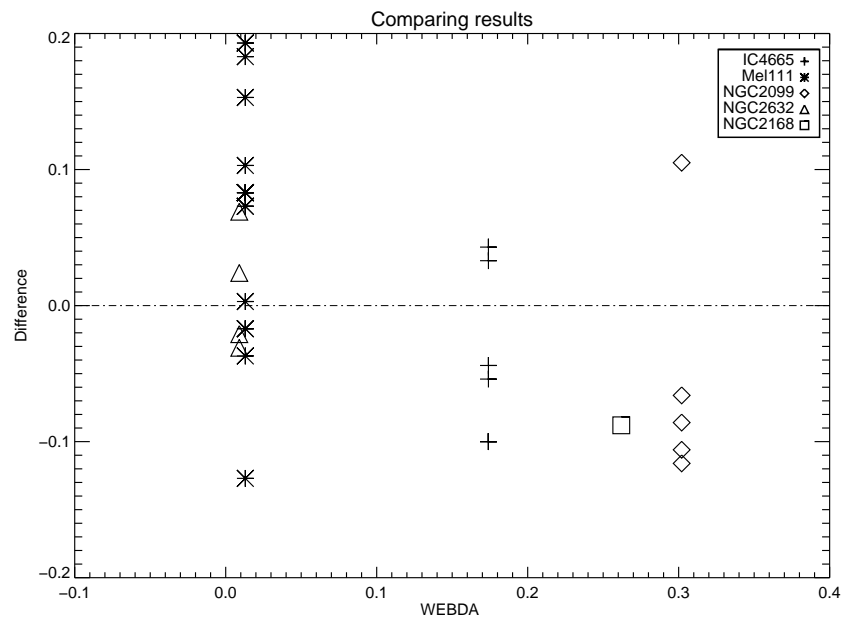


Figure 4.4: Absolute differences of reddening prediction when compared with WEBDA values (within 90% probability).

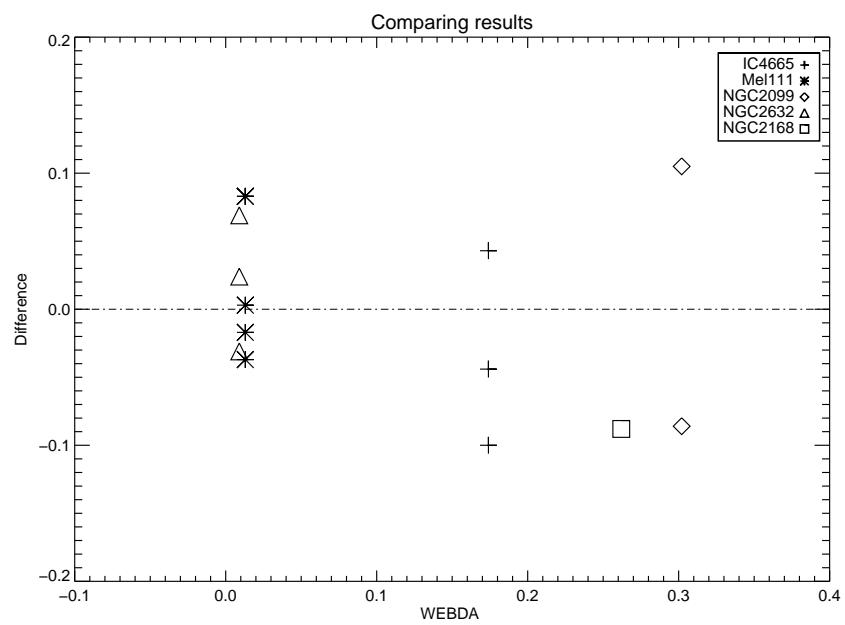


Figure 4.5: Absolute differences of reddening prediction when compared with WEBDA values (with maximum probability).

Chapter 5 Conclusions and recommendations

The aim of this research is to establish a method to measure interstellar reddening along any given line of sight. We have established a method that incorporates both spectral and photometric information to derive reddening along a line of sight up to a star. We find that our method is relatively accurate ($\sigma \Delta E(B - V) \approx 0.06$). This method does not suffer from resolution problem as in the case of SFD or any differential reddening problem as in color-color method.

At this moment we have used only 15 stars to make the conclusion. This is a low sample size to make a firm statistical conclusion. We therefore feel the necessity to get more sample to make the conclusion statistically robust. We also think to improve some of the procedures of the methods. Such as :

1. We have taken relatively small region of wavelengths ($\pm 70\text{\AA}$) to define the continuum. A larger region can help defining the continuum much more realistic.
2. The χ^2 statistics were done using the same part of the spectra as in continuum fitting. This can include some other lines and so can give erroneous results. We need to look carefully on the H β line only and try to avoid other possible spectral lines.
3. The reddening law that we used here is taken from Smith-Kaler (1998) and it is based on the extinction law where $R_V = 3.1$. We know that this is not a universal relation due to the non-uniform properties of dust grains. There are evidences where other reddening laws are reported (e.g., Bessell 1998)

Appendix A Stellar Spectral Lines

Spectral lines are the result of interaction between a quantum system (usually atoms, but sometimes molecules or atomic nuclei) and a single photon. When a photon has about the right amount of energy to allow a change in the energy state of the system (in the case of an atom this is usually an electron changing orbitals), the photon is absorbed. Then it will be spontaneously re-emitted, either in the same frequency as the original or in a cascade, where the sum of the energies of the photons emitted will be equal to the energy of the one absorbed (assuming the system returns to its original state). The direction and polarization of the new photons will, in general, correlate with those of the original photon.

Spectral lines in electromagnetic radiation originate when electrons make a transition from their initial state to a final state. They are the features imprinted on top of the continuum of the emitting source. There are emission lines and absorption lines. When electrons move from higher to lower energy state they emit radiation and so we get emission lines. On the other hand when electrons move from lower to higher energy they absorb radiation and we get absorption lines. These lines denote a particular physical phenomenon. All these lines show dynamical behavior that depends on the underlying physical condition such as temperature, pressure, surface gravity, metallicity etc. So by studying the spectral lines we can know much about the source that is emitting the radiation and also the material that is absorbing the radiation.

Natural Broadening: The uncertainty principle relates the lifetime of an excited state (due to the spontaneous radiative decay or the Auger process) with the uncertainty of its energy. This broadening effect results in an unshifted *Lorentzian* profile. The natural broadening can be experimentally altered only to the extent that decay rates can be artificially suppressed or enhanced.

Thermal Doppler Broadening: The atoms in a gas which are emitting radiation will have a distribution of velocities. Each photon emitted will be "red"- or "blue"-shifted by the Doppler effect depending on the velocity of the atom relative to the observer. The higher the temperature of the gas, the wider the distribution of velocities in the gas. Since the spectral line is a combination of all of the emitted radiation, the higher the temperature of the gas, the broader will be the spectral line emitted from that gas. This broadening effect is described by a *Gaussian* profile and there is no associated shift.

Pressure Broadening: the presence of nearby particles will affect the radiation emitted by an individual particle. There are two limiting cases by which this occurs:

Impact pressure broadening : The collision of other particles with the emitting particle interrupts the emission process. The duration of the collision is much shorter than the lifetime of the emission process. This effect depends on both the density and the temperature of the gas. The broadening effect is described by a Lorentzian profile and there may be an associated shift.

Quasistatic pressure broadening Quasistatic pressure broadening: The presence of other particles shifts the energy levels in the emitting particle, thereby altering the frequency of the emitted radiation. The duration of the influence is much longer than the lifetime of the emission process. This effect depends on the density of the gas, but is rather

insensitive to temperature. The form of the line profile is determined by the functional form of the perturbing force with respect to distance from the perturbing particle. There may also be a shift in the line center. A stable distribution is a general expression for the lineshape resulting from quasistatic pressure broadening

Pressure broadening may also be classified by the nature of the perturbing force as follows:

Linear Stark broadening occurs via the linear Stark effect which results from the interaction of an emitter with an electric field, which causes a shift in energy which is linear in the field strength. ($\Delta E \sim 1/r^2$)

Resonance broadening occurs when the perturbing particle is of the same type as the emitting particle, which introduces the possibility of an energy exchange process. ($\Delta E \sim 1/r^3$)

Quadratic Stark broadening occurs via the quadratic Stark effect which results from the interaction of an emitter with an electric field, which causes a shift in energy which is quadratic in the field strength. ($\Delta E \sim 1/r^4$)

Van der Waals broadening occurs when the emitting particle is being perturbed by van der Waals forces. For the quasistatic case, a van der Waals profile is often useful in describing the profile. The energy shift as a function of distance is given in the wings by e.g. the Lennard-Jones potential ($\Delta E \sim 1/r^6$).

Certain types of broadening are the result of conditions over a large region of space rather than simply upon conditions that are local to the emitting particle.

Opacity Broadening : Electromagnetic radiation emitted at a particular point in space can be absorbed as it travels through space. This absorption depends on wavelength. The line is broadened because photons at the line wings have a smaller re-absorption probability than photons at the line center. Indeed, the absorption near line center may be so great as to cause a self reversal in which the intensity at the center of the line is less than in the wings. This process is also sometimes called self-absorption.

Macroscopic Doppler Broadening : Radiation emitted by a moving source is a subject to the Doppler shift due to a finite line-of-sight velocity projection. If different parts of the emitting body have different velocities (along the line of sight), the resulting line will be broadened, with the line width proportional to the width of the velocity distribution. For example, radiation emitted from a distant rotating body, such as a star, will be broadened due to the line-of-sight variations in velocity on opposite sides of the star. The greater the rate of rotation, the broader the line. Another example is an imploding plasma shell in a Z-pinch.

Each of these mechanisms can act in isolation or in combination with others. Assuming each effect is independent, the observed line profile is a convolution of the line profiles of each mechanism. For example, a combination of the thermal Doppler broadening and the impact pressure broadening yields a *Voigt* profile.

However, the different line broadening mechanisms are not always independent. For example, the collisional effects and the motional Doppler shifts can act in a coherent manner, resulting under some conditions even in a collisional narrowing, known as the Dicke effect.

All objects in the sky has three dimensional motions. The projected motion in the sky (proper motion) and motion along the line of sight (radial motion). Due to the radial motion of the star we see Doppler effect. The spectral shift ($\Delta\lambda$) is related with radial velocity (V_r) as:

$$\Delta\lambda = \lambda \frac{V_r}{c} \quad (5.1)$$

where c is the speed of light and λ is the rest wavelength.

Appendix B Hydrogen Balmer Series

The Balmer series is characterized by the electron transitioning from $n \geq 3$ to $n = 2$, where n refers to the principal quantum number of the electron. The transitions are named sequentially by Greek letters α , β , γ , and δ . Transition from $n = 3$ to $n = 2$ is called $H\alpha$, from $n = 4$ to $n = 2$ is called $H\beta$, from $n = 5$ to $n = 2$ is called $H\gamma$, and from $n = 6$ to $n = 2$ is called $H\delta$ and H stands for hydrogen. The characteristic wavelengths of these transitions are 410 nm, 434 nm, 486 nm, and 656 nm respectively. All of them fall in the visible part of the electromagnetic spectrum and the colors corresponding to these wavelengths are red, cyan, blue and violet respectively.

In 1888 the physicist Johannes Rydberg generalized the Balmer equation for all transitions of hydrogen. The equation commonly used to calculate the Balmer series is a specific example of the Rydberg formula and follows as a simple reciprocal mathematical rearrangement of the formula above:

$$\frac{1}{\lambda} = R \left(\frac{1}{2^2} - \frac{1}{n^2} \right) \quad (5.2)$$

where R is the Rydberg constant and $n = 3, 4, 5, \dots$

The Balmer series is particularly useful in astronomy because the Balmer lines appear in numerous stellar objects due to the abundance of hydrogen in the universe, and therefore are commonly seen and relatively strong compared to lines from other elements. The spectral classification of stars, which is primarily a determination of surface temperature, is based on the relative strength of spectral lines, and the Balmer series in particular are very important. Other characteristics of a star can be determined by close analysis of its spectrum include surface gravity (related to physical size) and composition.

Because the Balmer lines are commonly seen in the spectra of various objects, they are often used to determine radial velocities due to Doppler shifting of the Balmer lines. This has important uses all over astronomy, from detecting binary stars, exoplanets, compact objects such as neutron stars and black holes (by the motion of hydrogen in accretion disks around them), identifying groups of objects with similar motions and presumably origins (moving groups, star clusters, galaxy clusters, and debris from collisions), determining distances (actually redshifts) of galaxies or quasars, and identifying unfamiliar objects by analysis of their spectrum.

Balmer lines can appear as absorption or emission lines in a spectrum, depending on the nature of the object observed. In stars, the Balmer lines are usually seen in absorption, and they are "strongest" in stars with a surface temperature of about 10,000 kelvin (spectral type A). In the spectra of most spiral and irregular galaxies, AGNs, H II regions and planetary nebulae, the Balmer lines are emission lines.

Bibliography

- Arce, H. G., and Goodman, A. A. 1999, ApJ, 512, 135
Beichman, C. A., and Jarrett, T. 1994, Ap&SS, 217, 207
Burstein, D. and Heiles, C., 1978, ApJ, 225, 40
Bellazzini, M., et al, 2004, MNRAS, 354, 1262
Bonifacio, P. et al., 2000, AJ, 120, 2065
Cambresy, L. et al., 2002, AJ, 123, 2559
Cambresy, L. et al., 2005, A&A, 435, 131
Clewley, L., et al., 2002, MNRAS, 337, 87
Drimmel, R., et al., 2003, A&A, 409, 205
Faber, S. M., et al., 1989, ApJS, 69, 763
Gray, R.O. and Corbally, C. J. 1994, AJ, 107, 742
Ibata, R. A., et al., 1997, AJ, 113, 634
Jarrett, T. H., Dickman, R. L., and Herbst, W. 1989, ApJ, 345, 881
Kurucz, R.L., 1993, <http://www.stsci.edu/hst/observatory/cdbs/k93models.html>
Lada, C. J., et al., 1994, ApJ, 429, 694
Lee, P., 2008, Tidal Streams in the Milky Way: An Observational Study (PhD Thesis)
Martin, N.F, et al., 2004, MNRAS, 348, 12
Momany, Y., et al., 2006, A&A, 421, 515
Neckel, Th., 1966, Z. Astrophys., 63, 221
Neckel, Th. and Klare, G., 1980, A&ASS, 42, 251
Schlegel, D. J. et al., AJ, 1998, 500, 525
Schultheis, M., et al., 1999, A&A, 349, 69
Schmidt-Kaler, T. 1982, in Landolt-Bornstein New Series, Group 6, Vol. 2b, Stars and Star Clusters, ed. K. Schaifers & H.-H. Voigt (Berlin: Springer)
White, S., Rees, M., 1978, MNRAS, 183, 341
Wolf, M., 1923, Astron. Nachr., 219, 185
Wood, D., Myers, P. C., and Daugherty D. A. 1994, ApJS, 95, 457

Vita

Date of Birth : 06-02-1976

Place of Birth : Dhaka, Bangladesh

Education: *Master of Science* in Advanced Techniques in Radio Astronomy and Space Science, Chalmers University of Technology, Sweden (2006)

Bachelor of Science in Mechanical Engineering, Bangladesh University of Engineering and Technology (2003)

Experience: *Research Assistant, Teaching Assistant*, Department of Physics and Astronomy, University of Kentucky (2006-2011)

Project Assistant, Hands on Universe, Europe (2005)

President, Bangladesh Astronomical Association (1997-1999)

Advisor, Planetarium project, Ministry of Science and Information & Communication Technology, Government of Bangladesh (1999)

Publications: *Thompson, G. et al*, Dust Emission from Unobscured Active Galactic Nuclei (Astrophysical Journal, 697, 182-193, 2009)

Uddin, S. et al, Seyfert 2 Mid-Infrared Spectral Signatures, With and Without Starbursts (Proceedings of the American Astronomical Society Meeting, Jan 7-11, 2008, Austin, TX)

Uddin, S., Few Astronomical Observations from Bangladesh (Proceedings of International conference on Physics for understanding and Applications; February 22-24, 2004, Dhaka)

Islam, S. et al, Appropriate low cost micro-hydro systems for Bangladesh (Proceedings of ICECE 2002, December 26-28, 2002, Dhaka)

Uddin, S., Performance study of a Solar PV water pumping system (Proceedings of Bangladesh Solar Energy Society, April 4-7, 2002, Dhaka)